

Substrate integrated Lead-Carbon hybrid ultracapacitor with flooded, absorbent glass mat and silica-gel electrolyte configurations

A BANERJEE^a, M K RAVIKUMAR^a, A JALAJAKSHI^a, P SURESH KUMAR^a,
S A GAFFOOR^b and A K SHUKLA^{a,*}

^aSolid State and Structural Chemistry Unit, Indian Institute of Science, Bangalore 560 012, India

^bNED Energy Limited, 6-3-1109/1, Navbharat Chambers, Raj Bhavan Road, Hyderabad 500 082, India

e-mail: akshukla2006@gmail.com

MS received 15 November 2011; revised 21 February 2012; accepted 12 March 2012

Abstract. Lead-Carbon hybrid ultracapacitors (Pb-C HUCs) with flooded, absorbent-glass-mat (AGM) and silica-gel sulphuric acid electrolyte configurations are developed and performance tested. Pb-C HUCs comprise substrate-integrated PbO₂ (SI-PbO₂) as positive electrodes and high surface-area carbon with graphite-sheet substrate as negative electrodes. The electrode and silica-gel electrolyte materials are characterized by XRD, XPS, SEM, TEM, Rheometry, BET surface area, and FTIR spectroscopy in conjunction with electrochemistry. Electrochemical performance of SI-PbO₂ and carbon electrodes is studied using cyclic voltammetry with constant-current charge and discharge techniques by assembling symmetric electrical-double-layer capacitors and hybrid Pb-C HUCs with a dynamic Pb(porous)/PbSO₄ reference electrode. The specific capacitance values for 2 V Pb-C HUCs are found to be 166 F/g, 102 F/g and 152 F/g with a faradaic efficiency of 98%, 92% and 88% for flooded, AGM and gel configurations, respectively.

Keywords. Hybrid ultracapacitor; substrate-integrated PbO₂ electrode; silica-gel electrolyte.

1. Introduction

Most ultracapacitors rely on carbon-based structures utilizing non-faradaic electrochemical-double-layer capacitance for charge storage. By contrast, pseudo-capacitive ultracapacitors are based on charge storage brought about by faradaic charge-transfer through surface adsorbed species. In the taxonomy of ultracapacitors, an ultracapacitor employing a non-faradaic double-layer electrode and a faradaic battery-type electrode is referred to as a hybrid ultracapacitor (HUC). HUCs are attractive as these could overarch the pulse power characteristics of an electrical-double-layer ultracapacitor and the sustained-energy characteristics of a battery. Accordingly, charge-storage mechanism in a hybrid ultracapacitor combines the mechanism of energy storage in a battery and a double-layer ultracapacitor. During the charge and discharge of a hybrid ultracapacitor, the battery type electrode undergoes charge-transfer through faradaic processes, namely oxidation and reduction, while the double-layer electrode undergoes non-faradaic processes, namely double-layer charge and discharge. HUCs have the benefits of both the batteries and ultracapacitors, namely

the high energy density of batteries and high power density with high cycle-life of ultracapacitors. Considering the technology need, availability, safety and cost, lead-carbon ultracapacitors are set to play a seminal role in future energy storage and management.

In the literature, Lead-Carbon ultracapacitors have been developed either by employing pasted positive plates of conventional lead-acid batteries or by employing electrochemically deposited PbO₂ on suitable substrates such as titanium as positive plates in conjunction with activated carbon as negative plates.^{1–8} The conventional pasted-type lead-acid battery electrodes require slow charge (C/10 rate) and discharge (C/5 rate) schedules for sustaining the desired cycle-life. Electrochemically deposited PbO₂ electrodes on a substrate, such as Ti, can be charged and discharged at much faster rates. However, these electrodes can store only limited amount of energy and hence exhibit lower energy and power density values besides being expensive. Furthermore, activated carbon electrodes used for such Pb-C HUC's reportedly employ a metallic substrate having protective coatings which could be prone to corrosion.⁹

In this study, novel cost-effective substrate-integrated PbO₂ positive plates are used to replace the conventional plates to circumvent the aforesaid problems. Lead sheets are used as substrate for positive plates

*For correspondence

that are subjected to electrochemical formation cycles during which a thin layer of PbO_2 is formed on the lead substrate. Since the substrate lead and electrochemically formed PbO_2 are integral part of the same electrode, the electrodes are termed as substrate-integrated PbO_2 (SI- PbO_2) positive plates. Such electrochemically formed substrate-integrated PbO_2 positive plates have several advantages over the conventional positive plates. In particular, SI- PbO_2 plates can be charged and discharged quickly with high faradaic efficiency and exhibit high cycle-life in addition to their high power density. SI- PbO_2 plates are easy to prepare and hence are cost-effective. Negative plates in Pb-C HUCs comprise electrical-double-layer-capacitor (EDLC) type electrodes obtained from activated-carbon-coated-graphite sheets. Since graphite is known to be a corrosion-resistant material such HUCs have high life-cycle. Among Pb-C HUCs with flooded, AGM and gel configurations reported here, Pb-C HUCs with gel configuration exhibit the best long-term performance.

2. Experimental

Details on preparation and characterization of SI- PbO_2 electrodes, electrical double-layer carbon electrodes, silica gel, and assembly of Pb-C HUCs are reported elsewhere.^{10,11} A brief account of these details is given below.

2.1 Preparation and characterization of polymeric silica-gel-electrolyte

Typically, 250 ml of silica-gel electrolyte was prepared from 5.5% (w/w) fumed silica by mixing 17 g of fumed silica with 100 ml de-ionized water to form a slurry followed by addition of 138 ml H_2SO_4 of density 1.4 g/cc and mechanical agitation. The surface area of fumed silica (M5 CAB-O-SIL[®]) was obtained from BET adsorption and desorption isotherm recorded on a BEL Inc. (Japan) Surface Area Analyzer and surface area was calculated by using 5320-Belsorp Adsorption/Desorption Data Analysis Software. FTIR spectrum for fumed silica was recorded on a Spectrum 1000 - Perkin Elmer FT-IR Spectrophotometer. X-ray diffraction pattern for fumed silica was recorded on a Philips X'pert-Pro X-ray diffractometer equipped with X'cellerator detector at scan speed ($^\circ/\text{s}$), step size ($^\circ$) and time per step values of 0.035, 0.016 and 30, respectively. The SEM image for the fumed silica was recorded using Sirion Scanning Electron Microscope

after gold coating. For TEM images dilute aqueous fumed silica suspension was drop casted on the carbon-coated copper grid. The measurements were carried out on a Technai T-20 TEM Microscope operating at 200 kV. Rheological properties of silica gel were studied using a stress-controlled Rheometer (Physica MCR 300-ANTONPAAR) employing a parallel geometry interfacial rheology cell with 0.05 mm separation between the two plates of 43 mm diameter.

2.2 Preparation and characterization of activated-carbon electrodes

Five wt.% of Poly(vinylidene fluoride) (PVDF) polymer was dissolved in required quantity of dimethylformamide (DMF) solvent by ultrasonication. Subsequently, 85 wt.% of high surface area ($\sim 1512 \text{ m}^2/\text{g}$) amorphous carbon (Meadwestvaco carbon X-090177) and 10 wt.% of activated charcoal AR ($\sim 974 \text{ m}^2/\text{g}$) (s d fine-chem Ltd., Mumbai 400 030, India) were dispersed into the PVDF-DMF solution to obtain a thick carbon-ink which was applied onto 0.3 mm thin graphite sheets with geometrical area of 63 ($4.5 \text{ cm} \times 7 \text{ cm}$) sq. cm and the tag dimensions of $1 \text{ cm} \times 1.5 \text{ cm} \times 0.3 \text{ mm}$. The geometrical area of the electrode (63 cm^2) was used to calculate the current density. Weight of the graphite electrode was $\sim 3 \text{ g}$. Each side of the electrode contained $\sim 0.5 \text{ g}$ carbon. Graphite electrodes were subsequently dried in an air oven at 80°C for 6–8 h. The electrodes were characterized by XRD and scanning electron microscopy. X-ray diffraction pattern for activated carbon electrode was recorded on the aforesaid instrument at scan speed ($^\circ/\text{s}$), step size ($^\circ$) and time per step values of 0.035, 0.016 and 30, respectively. SEM images for HUC electrodes were obtained on JEOL JSM-5600LV Scanning Electron Microscope. The carbon electrodes were assembled as symmetric electrical double-layer capacitors using 6 M aq. sulphuric acid or Absorbent glass-mat (AGM) in 6 M aq. sulphuric acid or silica gel with 1.4 g/cc aq. sulphuric acid for further characterization.

An Autolab Potentiostat/Galvanostat-Model 30 was used for electrochemical characterization of symmetric electrical-double-layer capacitors by cyclic voltammetry and constant-current charge-discharge. Single electrode potentials were recorded during charge and discharge of symmetric capacitor against a dynamic Pb (porous) / PbSO_4 reference electrode using a Keithley 2100 DMM Digital Multimeter interfaced with a computer.¹² The reference electrode exhibits a potential of -0.3 V vs. SHE. However, for the sake of convenience, all potentials are reported against SHE in the text.

2.3 Preparation and characterization of substrate-integrated PbO₂ electrodes

Substrate-integrated PbO₂ electrodes were prepared from lead sheets (99.9% purity) of dimensions 4.5 cm × 7 cm × 0.3 mm with tag dimension of 1 cm × 1.5 cm × 0.3 mm weighing ~ 15.4 g. Lead sulphate formed on the lead sheets after overnight dipping in 6 M aq. H₂SO₄ was converted to PbO₂ electrochemically. The electrodes thus obtained were characterized by XRD, XPS and scanning electron microscopy. X-ray diffraction patterns for Pb and PbO₂ were recorded on the above said powder X-ray diffractometer at scan speed (°/s), step size (°) and time per step values of 0.035, 0.016 and 30, respectively. X-ray photoelectron spectra (XPS) for the formed electrodes were obtained on a MultiLab 2000 Photoelectron Spectrometer from ThermoScientific, UK. SEM images for HUC electrodes were obtained on JEOL JSM-5600LV Scanning Electron Microscope. The capacity values for the electrodes were obtained by constant-current charge/discharge in 6 M aq. H₂SO₄ or AGM in 6 M aq. sulphuric acid or silica gel with 1.4 g/cc aq. sulphuric acid using carbon electrodes as counter electrodes.

2.4 Assembly and characterization of 2 V HUC prototype cells

2 V HUCs with an activated carbon electrode sandwiched between two SI-PbO₂ electrodes were assembled in 6 M aq. H₂SO₄ or AGM in 6 M aq. sulphuric acid or silica gel with 1.4 g/cc aq. sulphuric acid using a custom made Plexiglass cell for performance characterization. The weight ratio for the positive active material, negative active material and aq. sulphuric acid electrolyte in flooded HUCs was 1.6 : 1 : 32.5 while the

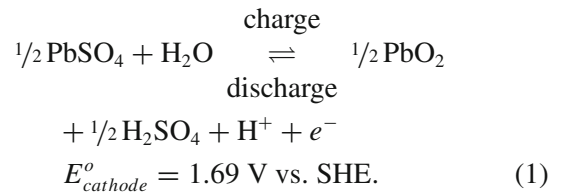
weight ratio for AGM and gel HUCs were 1.6: 1: 26 and 1.6: 1: 19.3, respectively. Performance tests on these cells were conducted by cyclic voltammetry, constant current charge-discharge curves and ac impedance.

3. Results and discussion

3.1 Operating principle of Pb-C HUC

In a Pb-C HUC, substrate-integrated PbO₂ electrodes are employed as cathode (-ve) and electrical double-layer carbon electrodes are employed as anode (+ve) with sulphuric acid as electrolyte. The operating principle of the Pb-C HUC is shown in figure 1. The PbO₂ electrode acts as battery electrode with the charge-discharge reactions similar to the positive plate (cathode) in a lead-acid battery. Accordingly, positive plate voltage in a Pb-C HUC is akin to the cathode of a lead-acid battery. The charge and discharge reactions for PbO₂ electrode and its voltage in HUCs can be written as follows.

At cathode:



In equation 1, $E_{\text{cathode}}^{\circ}$ is the standard electrode potential that changes with the concentration of the electrolyte. Accordingly, it is referred as E_{cathode} in the following text.

Activated carbon anode is an electrical-double-layer capacitor (EDLC). EDLC electrodes undergo only non-faradaic processes during charge and discharge and

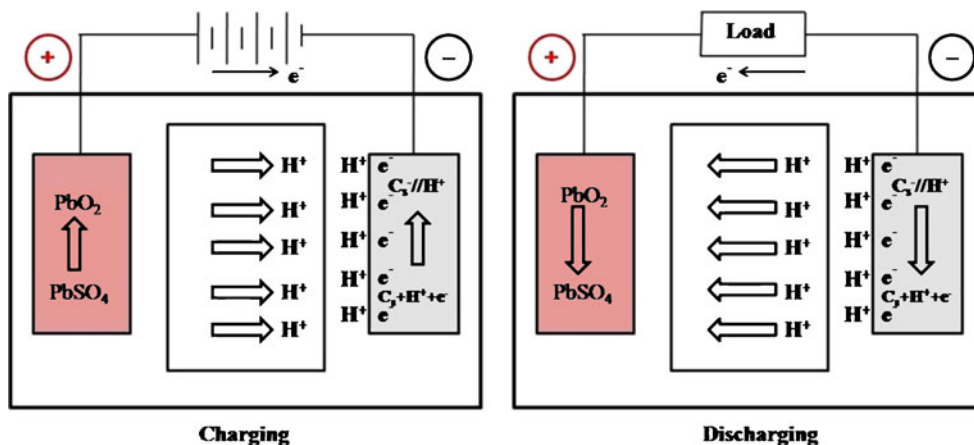
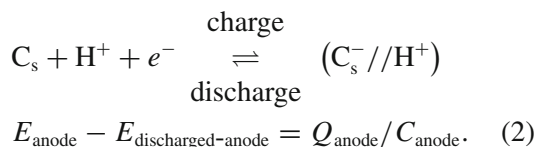


Figure 1. Charge-discharge schematic of a hybrid ultracapacitor.

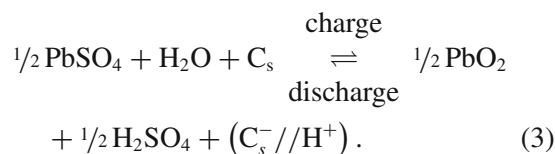
hence no thermodynamic equilibrium potential is established. The potential of the EDLCs depends on the total charge stored in the double layer. EDLCs are governed by the same physics as parallel-plate electrolytic capacitors but since EDLCs use much thinner dielectric medium and high surface-area electrodes, they tend to store relatively larger charge.¹³ The total charge (Q) stored in the double layer capacitor is proportional to its potential (V) with its capacitance (C) as proportionality constant, i.e., $Q \propto V$ or $Q = C V$. Accordingly, $V = Q/C$. The charge and discharge reactions on the activated carbon anode and its potential can be expressed as follows.¹⁴

At anode:



In equation 2, C_s represents the carbon atoms at the electrode surface, $//$ represents the double layer where charges are accumulated on either side, E_{anode} and $E_{\text{discharged anode}}$ refer to the potential of the electrode in its charged and discharged states, respectively, Q_{anode} is the charge on the carbon anode and C_{anode} is its capacitance in sulphuric acid electrolyte. The nature of interaction between C_s^- and H^+ is not yet established and is a subject of further study. However, the double layer behaviour of $C_s^-//H^+$ could be inferred

from ac impedance and cyclic voltammetry. The net cell reaction for Pb-C HUC is as follows.



The cell voltage is expressed as:

$$E_{\text{cell}} = E_{\text{cathode}} - (Q_{\text{anode}}/C_{\text{anode}}) \quad (4)$$

Accordingly, the cell voltage for Pb-C HUC depends on the anode capacitance and total charge on the carbon anode in sulphuric acid electrolyte.

3.2 Physicochemical characterization of SI-PbO₂ and carbon electrodes

X-ray diffraction patterns for activated carbon, Pb-metal plate used as substrate and substrate-integrated PbO₂ positive plate are shown in figure 2a, b and c, respectively. XRD pattern for the high surface-area carbon shown in figure 2a exhibits no sharp peaks but a broad peak at $2\theta = 22^\circ$ suggesting the carbon to be highly amorphous. XRD pattern for polished Pb-metal plate shown in figure 2b shows Pb crystallites to be in cubic phase. Figure 2c shows the lead metal plates subsequent to the formation process and consists of diffraction peaks for PbO₂ crystallites, predominantly

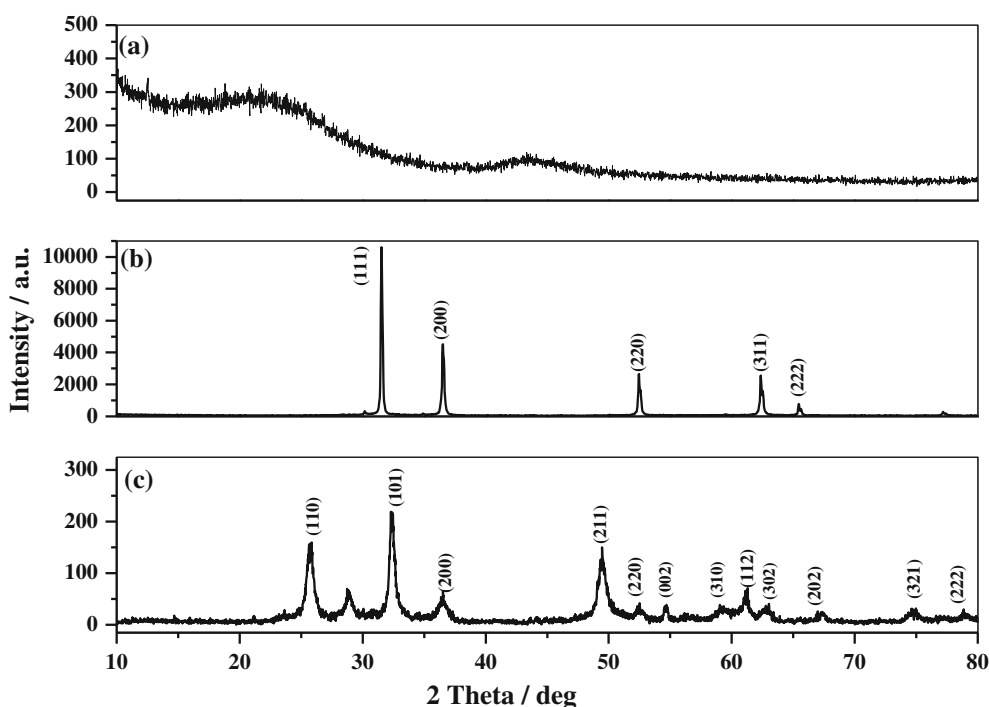


Figure 2. XRD patterns for (a) high surface-area-carbon, (b) pure lead-sheet, and (c) substrate-integrated lead dioxide.

in tetragonal β - PbO_2 phase, in addition to a peak at $2\theta = 28.6^\circ$ which is assigned to orthorhombic α - PbO_2 phase. The formation of both α - and β - PbO_2 phases with latter as predominant phase is in accordance with the literature.¹⁵ According to Petersson *et al.*,¹⁵ predominant formation of β - PbO_2 is a three-step process. In the first step, Pb is oxidized to form a mixture of PbO and PbSO_4 . Subsequently, PbO is oxidised to α - PbO_2 and PbSO_4 to β - PbO_2 in the second step. In the third and final step, α - PbO_2 is converted to β - PbO_2 .

SEM images for the carbon electrode, thin Pb-metal substrate and the Pb-metal electrode subsequent to the formation process are shown in figure 3a–f, respectively. SEM image for the carbon electrode in

figure 3a shows the electrode comprise uniformly distributed carbon particles. Figure 3b shows the SEM micrograph for polished metal plate and figure 3c shows the SEM micrograph of Pb-metal plate etched in 1M HNO_3 . The etched surface of the Pb-metal plate shows the formation of pits which increases the active surface area for the Pb-metal plate. Figure 3d shows the SEM image for SI- PbO_2 electrode. Figure 3e shows SEM image for the cross-sectional view of SI- PbO_2 electrode. Figure 3f shows the thickness for carbon coating to be about $300\ \mu\text{m}$ onto the graphite surface. Initially, a $300\ \mu\text{m}$ thick Pb-metal sheet is used as substrate and the thickness of these electrodes is found to increase to about $500\ \mu\text{m}$ after formation. The XRD

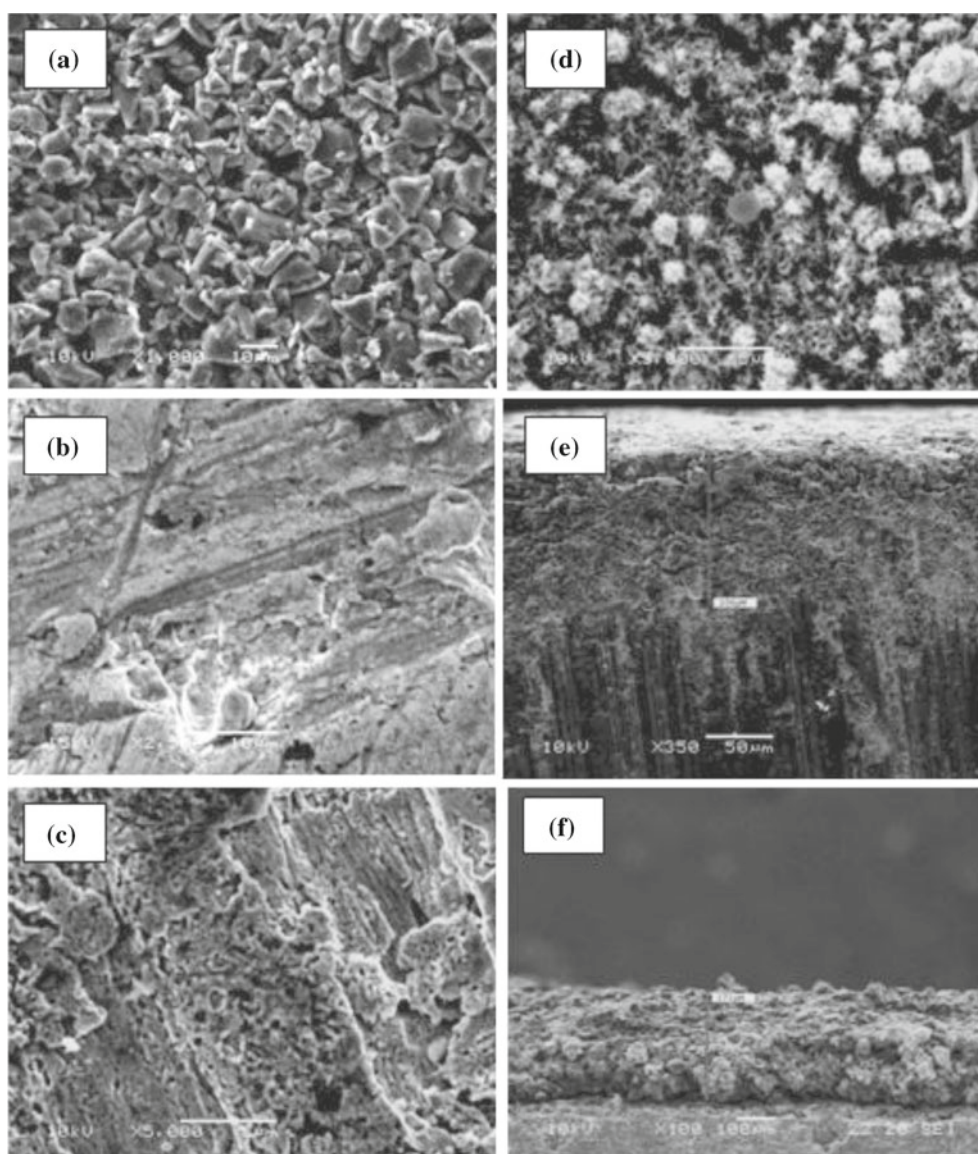


Figure 3. SEM images for (a) high surface-area-carbon, (b) lead sheet, (c) lead sheet after etching with nitric acid, (d) substrate-integrated PbO_2 , (e) cross-sectional view of substrate-integrated PbO_2 electrode, and (f) cross-sectional view of carbon coated graphite electrode. Scale bar: (a) $10\ \mu\text{m}$; (b) $10\ \mu\text{m}$; (c) $5\ \mu\text{m}$; (d) $10\ \mu\text{m}$; (e) $50\ \mu\text{m}$; (f) $100\ \mu\text{m}$.

pattern and SEM images for the Pb-metal plate prior and subsequent to its formation clearly indicate that a thin-layer of Pb-metal substrate is converted into PbO₂. The thickness of the PbO₂ is about 100 μm on either side of the electrode. XRD and SEM data on SI-PbO₂ electrode show the surface to be highly porous with the formation of PbO₂ crystallites. It is noteworthy that the earlier efforts to realize such substrate-integrated PbO₂ layers were not promising. In the O(1s) XPS spectrum of PbO₂, we find two peaks at 530.99 eV and 535.32 eV corresponding to O²⁻ and O₂²⁻ species with relative intensities of 2:1, respectively. ¹⁶Pb(4f_{7/2}) and Pb(4f_{5/2}) peaks found at 138.31 eV and 143.14 eV, respectively, are due to lead dioxide (see supplementary information: figure S1).

3.3 Physicochemical characterization of fumed silica

XRD pattern for the fumed silica shows a broad peak centered at $2\theta = 22^\circ$ indicating the fumed silica powder to be amorphous (see supplementary information: figure S2). Silica is a non-porous material but due to agglomeration of particles pores are generated. SEM image shows the presence of such pores (see supplementary information: figure S3). The particle size of fumed silica is found to be between 10–15 nm from TEM studies. Brunauer-Emmett-Teller (BET) adsorption-desorption method shows the nitrogen adsorption-desorption isotherm for fumed silica which is typical of a type II isotherm with type III hysteresis¹⁷ (see supplementary information: figure S4). The surface area for meso-structured fumed silica is found to be 166 m²/g with average pore-size of 20.5 nm. FTIR spectra shows peaks at about 3430 cm⁻¹, 1634 cm⁻¹, 1104 cm⁻¹, 810 cm⁻¹, and 472 cm⁻¹ for the fumed silica that are assigned to Si-OH stretching vibration, O-H bending vibration of adsorbed water molecule, asymmetric stretching vibration of Si-O-Si bond, Si-O bending vibration, and Si-O rocking vibration, respectively¹⁸ (see supplementary information: figure S5). It is surmised that fumed silica used to prepare the gel is in amorphous state with particles of 10–15 nm size. In solid form, silica particles are agglomerated with average pore size of 20.5 nm and surface area of 166 m²/g; it also has some adsorbed water molecules.

3.4 Rheological properties of silica gel

The rheological properties of silica gel, namely flow-curve, amplitude sweep and frequency sweep are obtained (see supplementary information: figure S6).

Viscoelastic gel exhibits resistance to flow under applied stress. The flow behaviour of gel is measured using simple rotational flow-curve experiment. The variation in viscosity (η) as a function of shear rate is also studied. With increasing shear rate ($d\gamma/dt$), the viscosity of silica gel decreases with a slope of -1.20 indicating silica gel to be a shear-thinning material. Fitting η vs. $(d\gamma/dt)$ with the power law equation: $\eta = m(d\gamma/dt)^{(n-1)}$, reveals $n < 1$ which implies the existence of 3D-network and suggests silica particles to be present in an attractive 3D-network in sulphuric acid medium. In an oscillatory amplitude sweep experiment, the storage modulus (G') represents the ability of the deformed material to restore its original geometry while the loss modulus (G'') represents the tendency of a material to flow under stress. Both G', G'' (Pa) are obtained as a function of increasing strain (%). The oscillation frequency is kept constant at 10 rad/s during the experiment. G', G'' vs. strain behaviour are characterized by a high value short plateau at lower strain corresponding to a linear viscoelastic (LVE) regime. In this regime for viscoelastic materials, like a gel, $G' > G''$, which demonstrates the elastic behaviour of the material. With increasing strain, the network structure is disrupted, and G' decreases and eventually becomes smaller than G'' . $G' = G''$ denotes the crossover strain at the point. The crossover strain for silica gel is 31.57% which indicates that the gel starts to flow above this value. In other words, the property of gel changes from a dominant elastic solid-like behaviour to a dominant viscous liquid-like behaviour. Dynamic rheology measurement is performed to further probe the gel characteristics. The experiment is performed under constant strain (0.1%), the magnitude of which is within the linear viscoelastic (LVE) regime. The frequency-independent response of G' and G'' demonstrates the stability of the gel over a wide range of time scales. Such behaviour is characteristic of a physical gel where silica particles are interconnected through physical bonds to form a space-filling network.¹⁹ The network responds elastically at small deformations and the generated stresses do not relax over the time period of the experiment.

3.5 Electrochemical characterization of electrical-double-layer carbon electrodes

HUCs comprise activated carbon and substrate-integrated PbO₂ electrodes. A complete performance characterization for both the carbon and substrate-integrated PbO₂ electrodes has been conducted prior to integrating them as HUCs. Figure 4a–c shows

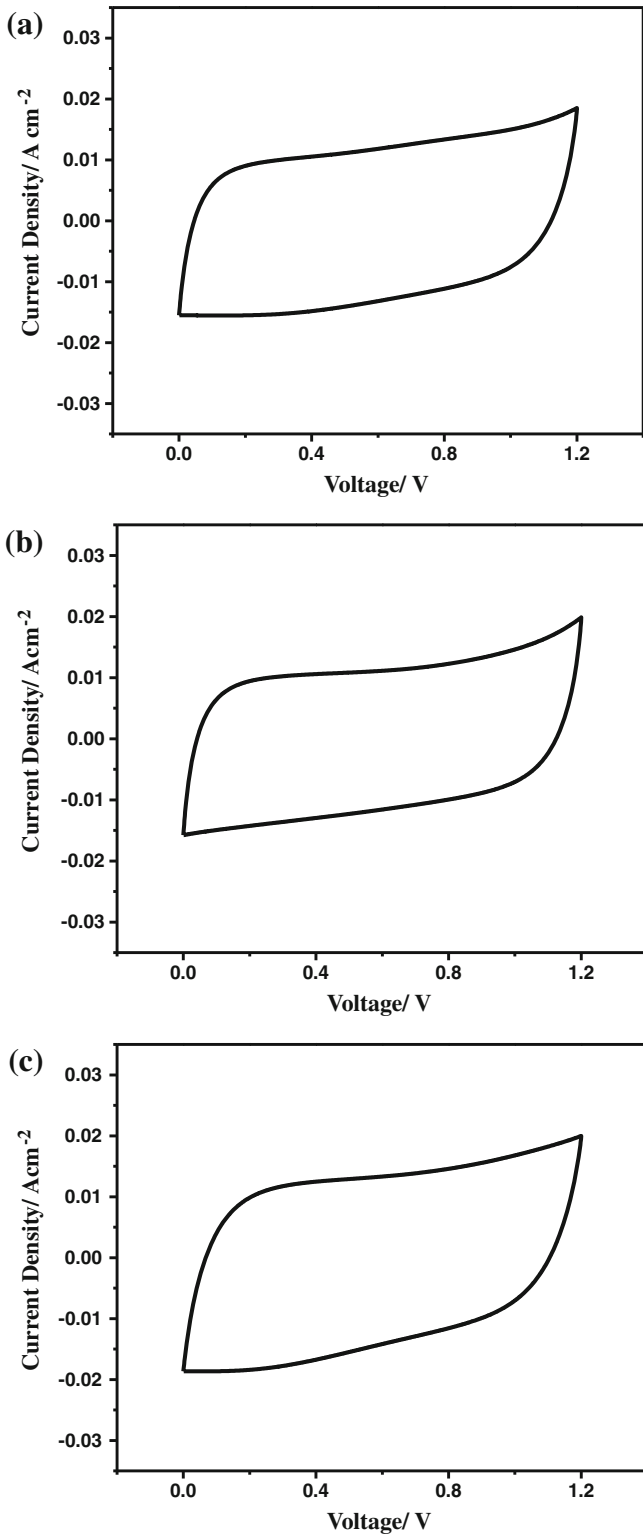


Figure 4. Cyclic voltammograms for MWV X-090177 carbon electrodes at scan rate of 10 mV/s in (a) flooded, (b) AGM and (c) gel electrolytes.

cyclic voltammograms for symmetric carbon capacitors in flooded, AGM and gel electrolyte configurations recorded in the potential range between 0 to 1.2 V at

the scan rate of 10 mV/s. During forward and reverse scans, no peaks are observed indicating that there are no oxidation or reduction reactions involved in forward and reverse scans. The observed current is assigned to the non-faradaic processes, such as double-layer charge/discharge. These cyclic voltammograms are typical of carbon-based EDLCs. Figure 5a–c shows the

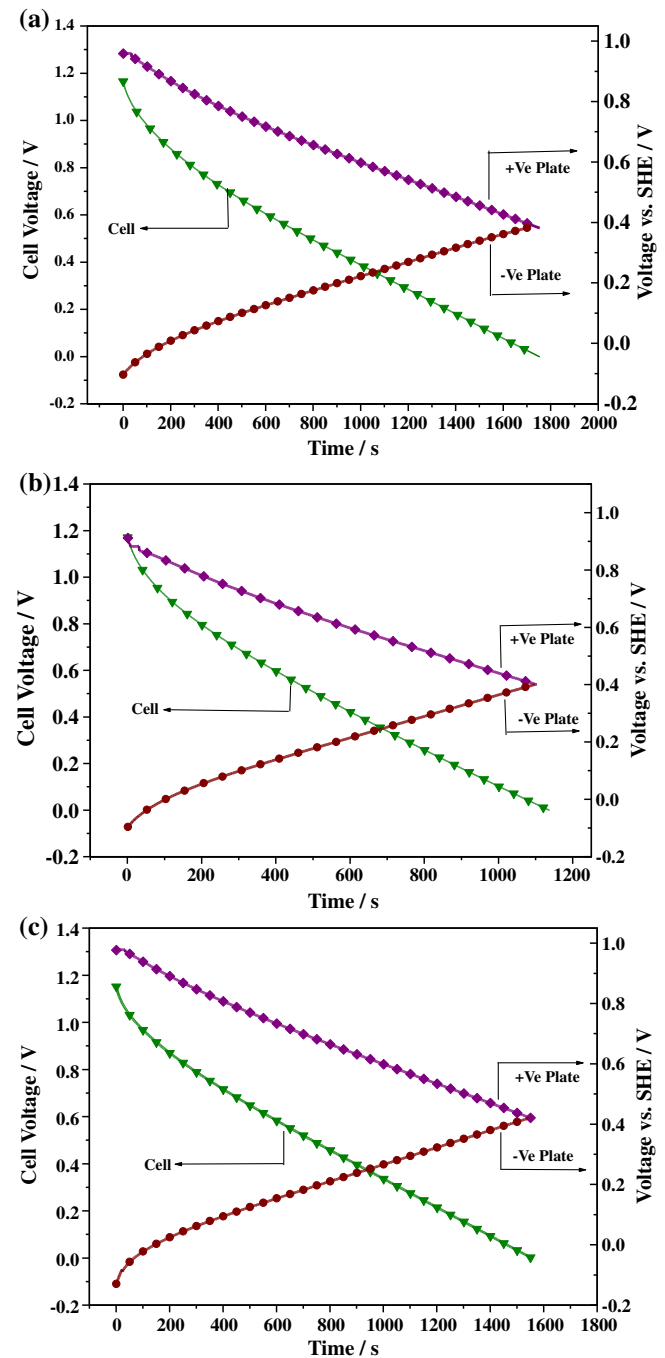


Figure 5. Constant-current discharge curves for symmetric carbon cell and single electrodes in (a) flooded, (b) AGM and (c) gel systems.

constant current discharge curves for symmetric carbon capacitors in flooded, AGM and gel electrolyte configurations. The single electrode potentials are also

shown in figure 5a–c. The single cell, anode and cathode capacitance values are obtained from the discharge curves of the symmetric capacitor. Since the symmetric

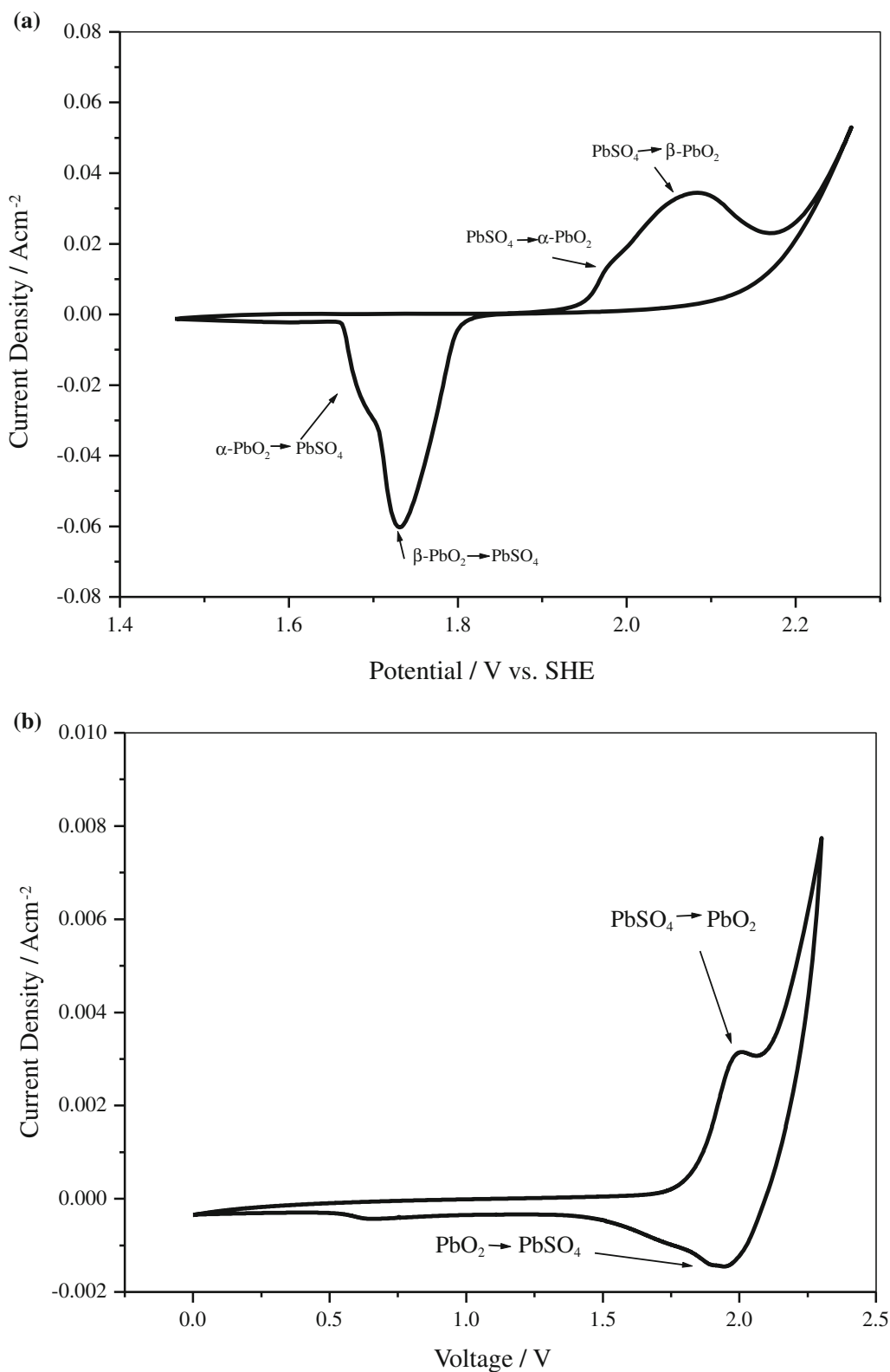


Figure 6. Cyclic voltammograms for (a) substrate-integrated lead electrode and (b) hybrid ultracapacitor single cell.

carbon ultracapacitors follow the principles of an electrolytic capacitor, the capacitance (C) of such ultracapacitors can be written as, $Q = C \times V$, where Q is the charge on the electrodes and V is the voltage difference between the electrodes.¹³ Since $Q = I \times t$, where I and t represent current and time, respectively, one can express: $V = \frac{I \times t}{C}$, and on differentiating the voltage of such capacitors with respect to time at constant current, we get, $\frac{dV}{dt} = \frac{I}{C}$.

During the constant current charge/discharge of such ultracapacitors, voltage varies linearly with time. The charging curves have positive slope of I/C while discharge curves have negative slope of $-I/C$. In practice, during the discharge of an ultracapacitor, there will be an initial voltage drop due to the internal ohmic resistance, referred to as IR drop, where R represents the ohmic resistance. Since this voltage drop is not available for capacitive discharge, the capacitance is calculated excluding both ESR (equivalent series resistance) and EDR (electrical double-layer resistance). We have calculated the capacitance of single cell, anode and cathode from the aforesaid equations and it is found that the symmetric carbon capacitors have respective total capacitance values of 71 F/g, 48 F/g and 65 F/g for flooded, AGM and gel configurations at a discharge

current density of 1.6 mA cm^{-2} that corresponds to 100 mA of discharge current. The discharged capacitor is charged galvanostatically at 1.6 mA cm^{-2} to the cut-off voltage of 1.2 V and subsequently charged potentiostatically at 1.2 V for 5 min to ensure that it is fully charged.

Since the symmetric capacitor comprises two electrode-electrolyte interfaces, the symmetric carbon capacitor can be represented as two capacitors connected in series, namely a capacitor at the anode-electrolyte interface and the other at the cathode-electrolyte interface. The net capacitance for two capacitors connected in series can thus be written as: $\frac{1}{C_T} = \frac{1}{C_{\text{anode}}} + \frac{1}{C_{\text{cathode}}}$, where C_T is the total capacitance, C_{anode} is the capacitance due to anode-electrolyte interface and C_{cathode} is the capacitance due to cathode-electrolyte interface. Accordingly, capacitance values for the individual electrodes are obtained from the discharge curves for the symmetric carbon capacitor and it is found that the double-layer capacitance at the anode-electrolyte interface is 328 F/g while the double-layer capacitance due to cathode-electrolyte interface is 270 F/g for flooded EDLC. This shows that the symmetric carbon capacitors indeed have an intrinsically asymmetric capacitance. This is mainly due to the nature

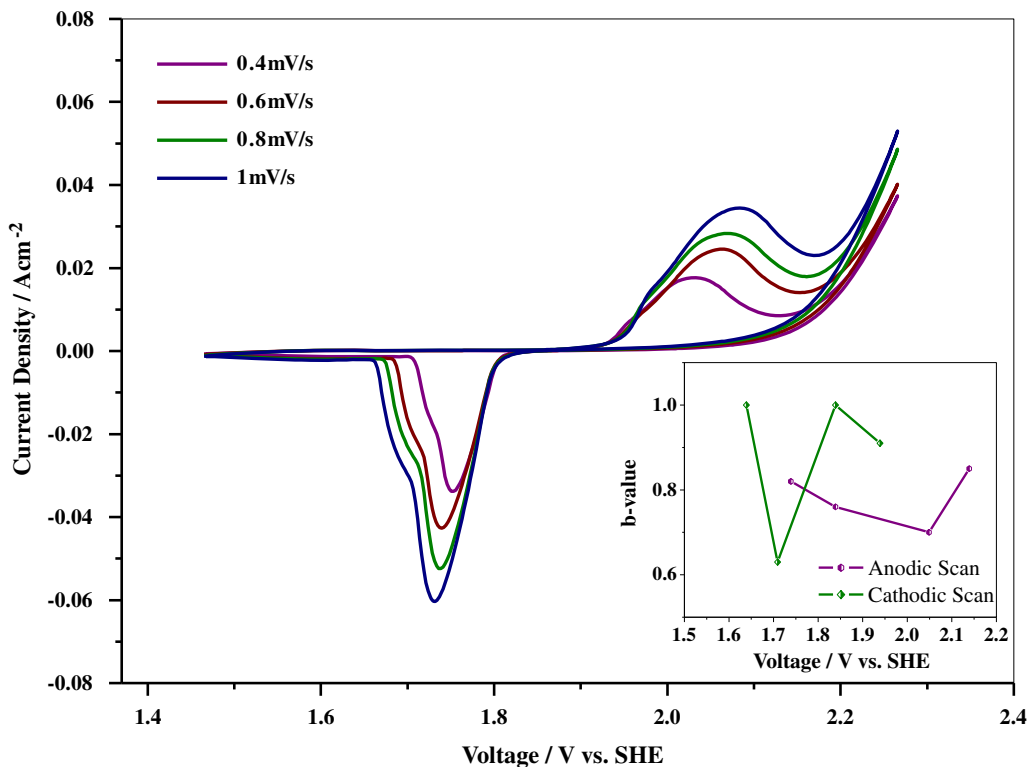


Figure 7. Cyclic voltammograms for substrate-integrated PbO_2 electrode at varying scan rates. Inset: calculated b-values for a substrate-integrated PbO_2 electrode as a function of potential for the anodic and cathodic sweep.

of the ions that are present in the respective double layers at the electrode-electrolyte interfaces¹. The specific capacitance is obtained from the weight of the carbon. The specific capacitance of the symmetric carbon capacitor with flooded electrolyte is measured to be 71 F/g while measured specific capacitance values for anode and cathode are 328 F/g and 270 F/g, respectively. Accordingly, the calculated value of the specific capacitance for the symmetric carbon capacitor with flooded electrolyte is 74 F/g. For AGM and gel electrolyte symmetric carbon capacitors, the specific capacitance for the symmetric carbon capacitors are 48 F/g and 65 F/g, respectively. The specific anode and cathode capacitance values for AGM system are about 237 F/g, 212 F/g, respectively. Similarly, for the gelled electrolyte capacitor, the specific capacitance values for anode and cathode are about 283 F/g, and 268 F/g, respectively. It is noteworthy that the degree of utilization for carbon surface area in the flooded, AGM and gelled electrolyte configurations varies as flooded > gelled > AGM and hence the respective capacitance values.

From the Stern model for the electrical double-layer, the total double-layer capacitance is expressed as the series combination of capacitances arising due to Helmholtz (compact) double-layer and diffused double-layer. The capacitance of the Helmholtz layer, C_H , is usually smaller than the diffused double-layer, C_{diff} , primarily due to the difference in their thickness. Accordingly, the total capacitance observed, C_{obs} , is determined from the equation:

$$1/C_{obs} = 1/C_H + 1/C_{diff} \sim 1/C_H \quad (C_H \ll C_{diff}). \quad (5)$$

The polymeric component in the electrolyte directly influences the C_H value. The capacitance of the Helmholtz layer is determined by its thickness and permittivity of the medium, both of which are quite different for the electrolytes with and without the polymeric component. In the light of the foregoing, it is highly likely for the capacitance of the gelled polymer electrolyte configuration to be higher than the AGM configuration.²⁰

3.6 Electrochemical characteristics of 2 V Pb-C HUCs

3.6a Cyclic voltammetry: Cyclic voltammogram for substrate-integrated PbO₂ electrode in 2 V Pb-C HUC, assembled in 6 M aq. H₂SO₄ electrolyte at 1 mV/s scan rate is shown in figure 6a. The voltammogram for substrate-integrated PbO₂ electrodes is similar to

the conventional PbO₂ positive electrodes in a lead-acid battery. The anodic voltammetric curve shows two peaks designated as I and II. Peak I observed at about 1.97 V vs. SHE is assigned to the formation of α -PbO₂ from PbSO₄ and peak II observed at 2.08 V vs. SHE is assigned to formation of β -PbO₂ from PbSO₄.²¹ The cathodic scan voltammogram shows peaks for

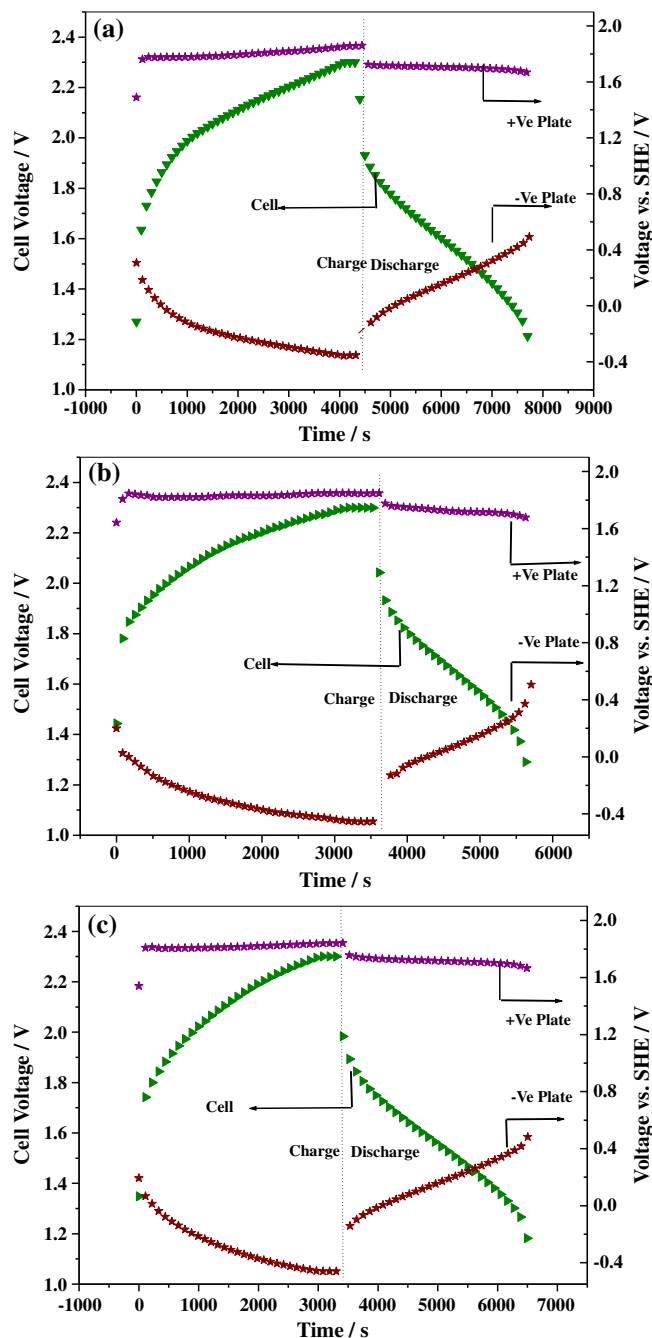


Figure 8. Galvanostatic charge followed by potentiostatic charge and galvanostatic discharge for 2 V Pb-C HUCs with single electrode charge-discharge profiles for (a) flooded, (b) AGM, (c) gel configurations.

reduction of α - and β - PbO_2 from PbSO_4 at 1.68 V and 1.73 V, respectively.

A typical cyclic voltammogram for substrate-integrated Pb-C HUC with flooded 6 M aq. H_2SO_4 electrolyte at 1 mV/s scan rate is shown in figure 6b. Voltammogram for the hybrid ultracapacitor single cell shows voltammetric peaks akin to substrate-integrated PbO_2 electrodes shown in figure 6a. However, the anodic peak assigned to the oxidation of PbSO_4 to PbO_2 is now observed at 2 V. The cathodic peak corresponding to reduction of PbO_2 to PbSO_4 is observed at 1.94 V.

Cyclic voltammograms for the SI- PbO_2 electrodes, carbon electrode and the HUCs clearly show that HUC is a combination of a battery type electrode and an EDLC electrode. The charge storage in the SI- PbO_2 electrode is through faradaic charge-transfer-reaction via oxidation of PbSO_4 to PbO_2 and reduction of PbO_2 to PbSO_4 as represented by equation 1.

Since the presence of non-faradaic component with SI- PbO_2 cannot be completely ruled out, an effort is made to separate faradaic and non-faradaic capacitances associated with the SI- PbO_2 electrode. Figure 7 shows the cyclic voltammogram for SI- PbO_2 electrode at varying scan rates between 0.4 mV/s and 1 mV/s. The area under the curve represents the total stored charge

originating from faradaic and non-faradaic processes. The faradaic and non-faradaic components could be accounted using the power law: $i = av^b$ where v is scan rate, and both a and b are adjustable parameters. The parameter b is determined from the slope of linear plot of $\log i$ vs $\log v$. In general, slope $b = 1$ for surface capacitive component involving non-faradaic processes where $i = av$, while for an ideal faradaic process, slope $b = 1/2$ which leads to Cottrell's equation: $i = av^{1/2}$. The analysis of the anodic and cathodic sweep data suggests the non-faradaic and faradaic components to be about 43% and 57%, respectively.^{22,23}

The charge storage mechanism for the carbon electrode is through non-faradaic charge and discharge of the electrical double layer as shown in equation 2. Hence, the charge storage mechanism in Pb-C HUCs is a combination of the two processes as shown in equation 3. Accordingly, hybrid ultracapacitors are potential devices with the benefits of both the batteries and ultracapacitors.

3.6b *Constant-current and constant-potential charge and constant-current discharge characterization for 2 V substrate-integrated Pb-C HUC single cells:* Constant current and constant potential charge–constant current

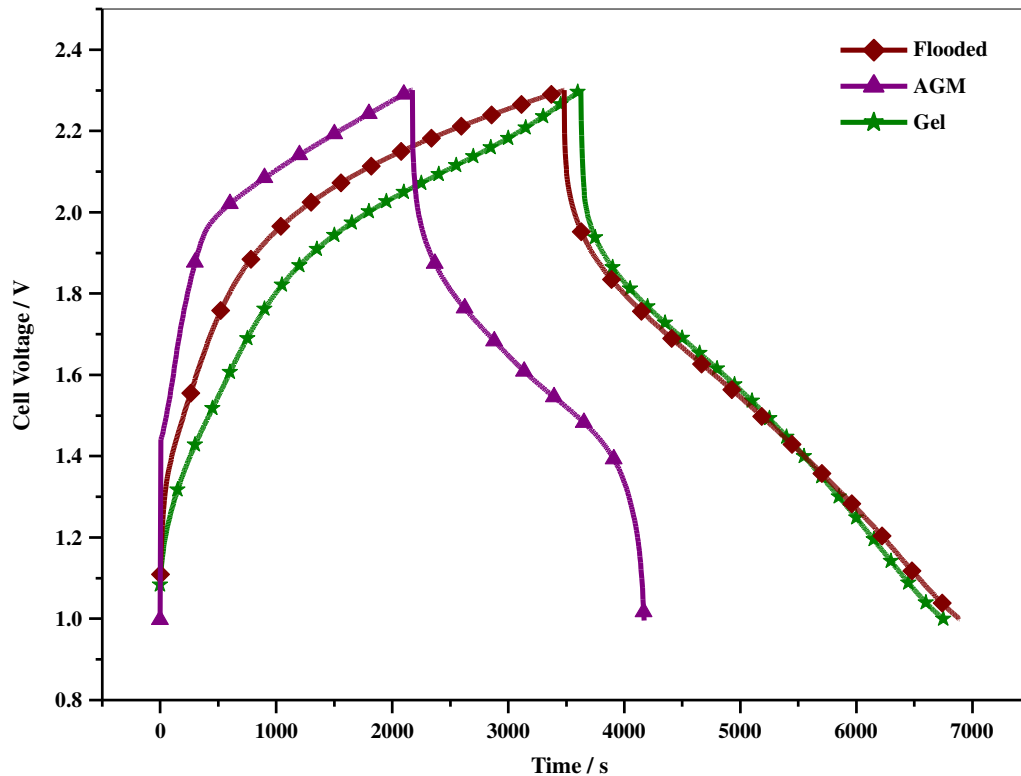


Figure 9. Comparison of constant-current charge and discharge data for 2 V Pb-CHUCs.

discharge data for 2 V substrate-integrated Pb-C HUC single cells at 1.6 mA cm^{-2} (corresponding current = 100 mA) are shown in figure 8a–c along with single electrode charge–discharge curves in flooded, AGM and gel electrolytes. The open-circuit voltage for the fully-charged cell is $\sim 2.1 \text{ V}$ for flooded and AGM configurations and $\sim 2 \text{ V}$ for gel configuration. All the capacitors are discharged to a cut-off voltage of 1.15 V. It is clearly seen that the charge-discharge data for the substrate-integrated PbO_2 electrode are akin to the conventional lead-acid battery positive electrode while charge-discharge data for carbon electrode are similar to the anodic charge-discharge curve of the symmetric capacitor electrode as shown in figure 5a–c. The discharge curve voltage for the substrate-integrated Pb-C HUC single cell decreases gradually during the discharge after an initial voltage drop due to internal resistance of the cell. The cell voltage drops steeply at about 1.15 V at the end-of-discharge. The single electrode potential for the substrate-integrated PbO_2 electrode during its charge and discharge remains almost constant as in a conventional lead-acid battery. However, the single electrode potential for the capacitor type carbon anode changes from -0.34 V to 0.52 V , -0.44 V to 0.51 V and -0.44 V to 0.51 V vs. SHE for the flooded, AGM and gel configurations, respectively, during the discharge. Accordingly, during the discharge of the substrate-integrated Pb-C HUC single cell, the voltage decreases mainly due to the capacitor type carbon anode.

Constant current charge and discharge curves for substrate-integrated Pb-C HUC single cells with flooded, AGM, gelled configurations at 1.6 mA cm^{-2} current density are shown in figure 9. The cells are charged to the cut-off-voltage of 2.3 V and subsequently discharged to the cut-off-voltage of 1 V. The faradaic efficiency values calculated from these data are found to be 98%, 92% and 88% for flooded, AGM, gel configurations, respectively. In the gelled system various parasitic reactions are possible due to enhanced surface area of the positive plate as reflected by the lower faradaic efficiency.

All the three kinds of HUC single cells are performance tested by constant current discharge at varying current loads and the data are shown in figure 10a–c. Overall specific capacitance values for flooded, AGM and gel HUCs are found to be 166 F/g, 102 F/g and 152 F/g, respectively, at 1.6 mA cm^{-2} discharge current density after galvanostatic charge followed by 5 min potentiostatic charge at 2.3 V. It is clearly seen that the flooded and gel electrolyte HUCs exhibit higher capacitance than the AGM-based HUC. The specific capacitance values are found to be 132 F/g, 51 F/g and

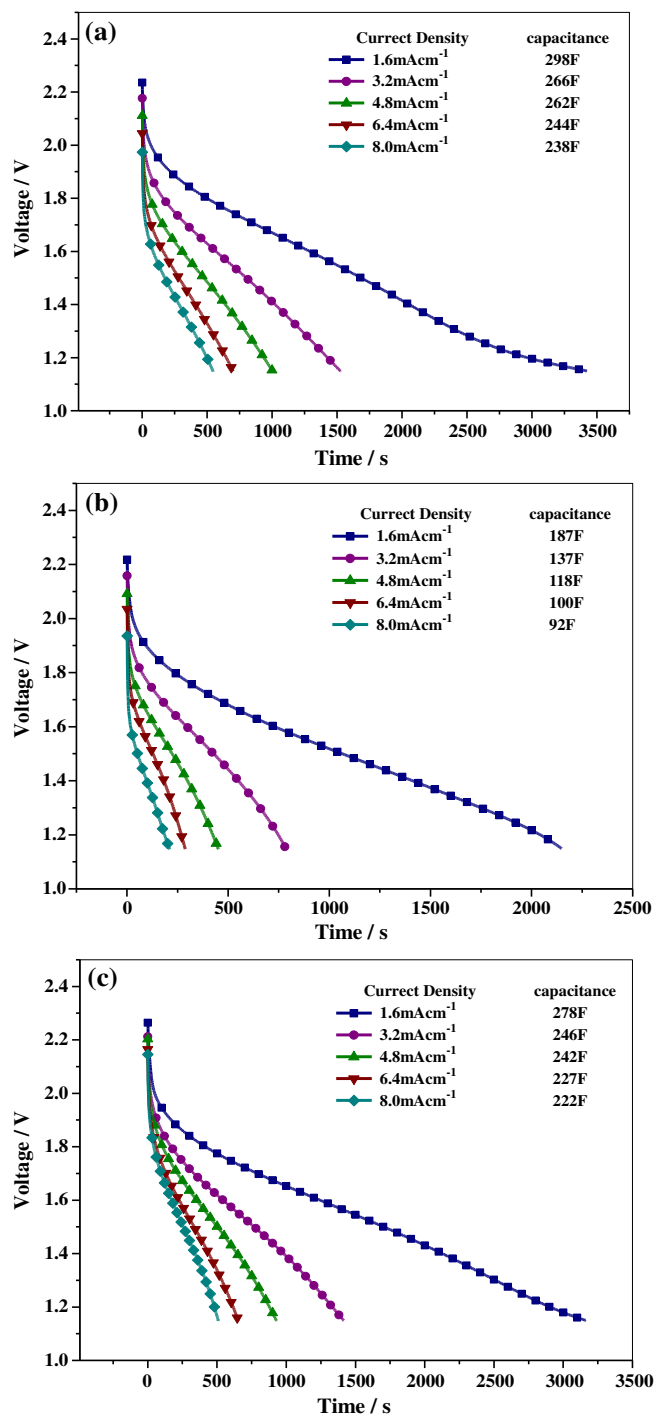


Figure 10. Constant current discharge data for 2 V Pb-C HUC at varying discharge current-loads for (a) flooded, (b) AGM, and (c) gel HUCs.

123 F/g at a discharge current density of 8 mA cm^{-2} (current = 500 mA) for flooded, AGM and gelled cells, respectively. The change in the capacitance of the SI- PbO_2 HUC is mainly attributed to the differential capacitive behaviour of the carbon anode as the discharge curves for the SI- PbO_2 electrode remain flat at all the discharge current densities.²⁴

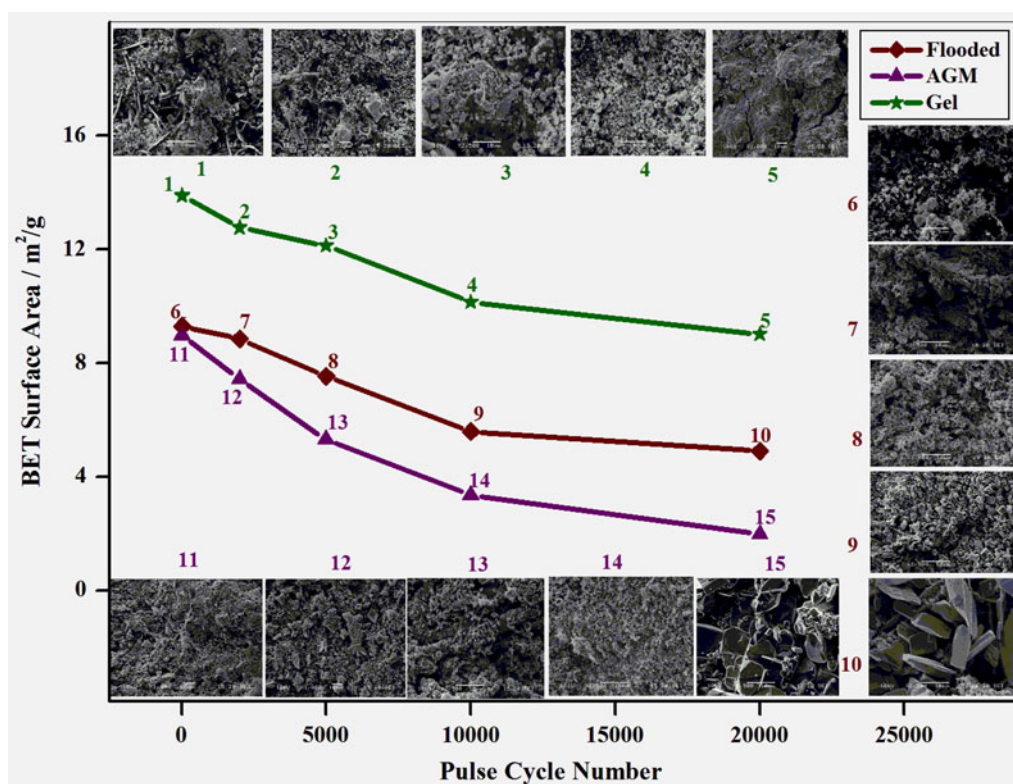


Figure 11. Effect of pulsed charge and discharge cycling on the surface area of SI-PbO₂ during cycling.

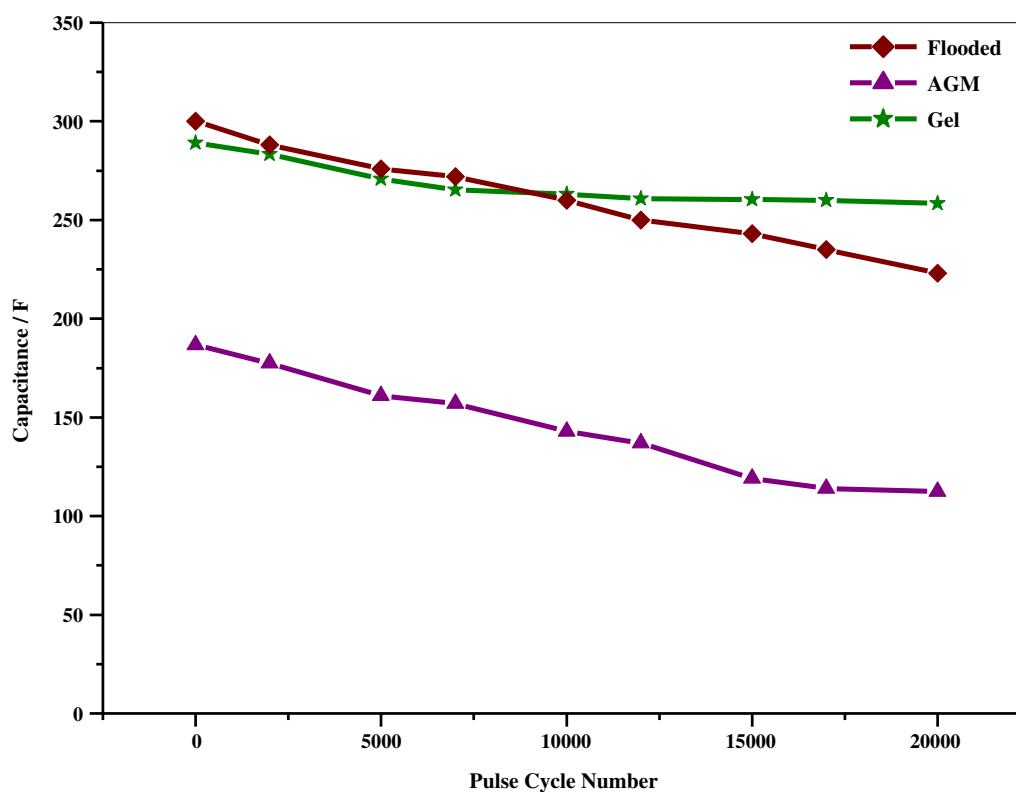


Figure 12. Effect of pulsed charge and discharge cycling on the capacitance for HUCs.

Table 1. Leakage current and self-discharge data for flooded, AGM and gel electrolyte 2 V Pb-Carbon HUCs.

Device	Parameter	Flooded	AGM	Gel
2 V Lead–Carbon HUCs	Leakage current/mA	8	11	15
	Parallel resistance/ Ω	1669	209	155
	Self-discharge at room temperature (28 °C) / %	18	19	28

3.6c Role of silica gel in Pb–C HUCs: In the flooded-electrolyte configuration, higher surface area of the electrodes is exposed to electrolyte than AGM and gel electrolyte configurations yielding higher capacitance for the former. Between the AGM and gel configurations, appreciable increase in the surface area of the active material for the lead dioxide electrode is observed for gel configuration providing higher capacitance for the latter. Silica particles appear to have distinct role in controlling the nucleation of PbO_2 on positive plate during electrochemical formation.²⁵ Silica particles affect the nucleation process of PbO_2 and control its particle size. Accordingly, in the gel electrolyte, the particle size of PbO_2 is smaller than AGM yielding higher surface area and porosity. In order to establish the role of silica gel on the capacitance of HUCs, a detailed study is carried out by measuring the initial surface area of SI- PbO_2 and then cycling the HUC (figure 11). Initially, the active material for a SI- PbO_2 electrode has a BET surface area of 7.3 m^2/g . It is noteworthy that prior to the BET measurement, it is ascertained from XRD that PbO_2 has no metallic lead. A gel HUC with above mentioned SI- PbO_2 electrode is subjected to slow charge-discharge at 1 mA/cm^2 for 10 cycles in the voltage window between 1.15 V and 2.3 V. For the BET measurements, after every complete charge, SI- PbO_2 electrode is taken out from the capacitor and is copiously washed with de-ionized water followed with acetone and active material is collected. The surface area of the PbO_2 active material in gel configuration is found to be 13.9 m^2/g , whereas its value in the AGM configuration is $\sim 9 \text{ m}^2/\text{g}$. The enhancement in BET surface area for PbO_2 in the gel configuration facilitates higher capacitance as compared to the AGM configuration.

3.6d Self-discharge, leakage current and parallel resistance characteristics of 2 V Pb-C HUCs: Self-discharge is an important parameter of any capacitor. In the present study, self-discharge for the HUC is measured after charging them potentiostatically for

1h at 2.3 V followed by 24 h in open-circuit condition. It is observed that self-discharge for the gelled configuration is higher than the flooded and AGM configurations. As the self-discharge is higher for gelled system, the leakage current also is higher while parallel resistance is lower for it. Leakage current is also measured during 24 h after fixing the voltage at 2.3 V. Parallel resistance after 24 h is obtained as a ratio of working voltage, i.e., 2.3 V, and leakage current after 24 h. Self-discharge, leakage current and parallel resistance values for flooded, AGM, gel single cell HUCs are given in table 1²⁶. It is noteworthy that the enhancement in BET surface area for PbO_2 active material adds up to self-discharge of HUC in gel configuration (see supplementary information: figure S7).

3.6e Pulsed charge-discharge studies for 2 V Pb-C HUCs: HUCs in various electrolyte configurations are subjected to pulsed charge-discharge cycles of 1A for duration of 1 s followed by 5 s rest. The BET surface area for the SI- PbO_2 in HUCs subsequent to 2,500, 5,000, 10,000 and 20,000 pulses are obtained and their capacitance values measured as a function of cycle number shown in figures 11 and 12. Gel HUC shows the best cycling performance as compared to flooded and AGM HUCs. After repeated charge-discharge cycles, the particle size of PbO_2 increases lowering its BET surface area as shown in figure 11.

3.6f Impedance characteristics for 2 V Pb-C HUCs: It is well established from Bode plot (phase vs. frequency) that the resistance and capacitive reactance are equal at -45° ; the corresponding frequency being named as breaking frequency. After this point capacitive reactance become larger than resistance. The time corresponding to the breaking frequency is named as response time of the capacitor. The response times for the HUCs are estimated to be 1.33 s, 1.44 s and 2.05 s for the flooded, AGM and gel electrolyte configurations, respectively (see supplementary information: figure S8).

4. Conclusions

Pb-C HUCs comprising substrate-integrated PbO₂ electrodes as battery-type positive electrode and electrical-double-layer type carbon as negative electrode with flooded sulphuric acid, absorbent glass-mat and silica gel electrolytes are developed and performance tested. The capacitance of electrical double-layer type carbon electrodes, capacity of the SI-PbO₂ and performance of the Pb-C HUCs are found to be sensitive to various electrolyte configurations, namely flooded, AGM and polymeric silica-gel sulphuric acid. The specific capacitance of the carbon used in this study is found to be 71 F/g, 48 F/g and 65 F/g for flooded, AGM and gel configurations at a discharge current density of 1.6 mA cm⁻² (corresponding current = 100 mA). The specific capacitance values for anode and cathode are also calculated from single electrode potential measurements. It is found that the anode capacitance is 328 F/g, 237 F/g and 283 F/g, respectively, for flooded, AGM and silica gel sulphuric acid electrolyte configurations. Similarly, the cathode capacitance is found to be 270 F/g, 212 F/g and 268 F/g, respectively, for the flooded, AGM and silica gel sulphuric acid electrolyte configurations. The high capacitance obtained for the flooded and silica gel electrolyte configurations is mainly attributed to the higher utilization of carbon surface area in relation to the AGM-based sulphuric acid electrolyte configuration. The difference in anode and cathode capacitance is attributed to the intrinsic nature of the ions involved in the formation of double layer. Cyclic voltammetric studies on the 2 V Pb-C HUCs clearly reveal novel feature of charge storage in these hybrid ultracapacitors. It is found that these HUCs store charge through a combination of faradaic charge transfer processes associated with the reduction and oxidation of PbO₂ electrode, and non-faradaic charge and discharge processes of electrical double layer associated with carbon electrode. Specific capacitance values of 166 F/g, 102 F/g and 152 F/g with a faradaic efficiency of 98%, 92% and 88% are found for flooded, AGM and silica gel 2 V Pb-C HUCs, respectively. The BET surface area of 7.3 m²/g obtained for PbO₂ is found to increase to 9 m²/g and 13.9 m²/g for AGM and silica-gel electrolytes, respectively, after 10 cycles of charge and discharge. The higher capacitance for silica gel system is attributed to the higher surface area of the active material in the HUCs. In the silica gel system various parasitic reactions are possible due to enhanced surface area of the positive plate as reflected by its lower faradaic efficiency.

Supplementary information

The electronic supporting information (figures S1–S8) can be seen in www.ias.ac.in/chemsci.

Acknowledgements

Financial support from the Department of Science and Technology, Government of India, and Indian Institute of Science, Bangalore under its Energy Storage systems Initiative is gratefully acknowledged. AB thanks the Council of Scientific and Industrial Research (CSIR), New Delhi for a Junior Research Fellowship.

References

- Pell W G and Conway B E 2004 *J. Power Sources* **136** 334
- Zhou D and Gao L 2007 *Electrochim. Acta* **53** 2060
- Yu N and Gao L 2009 *Electrochem. Commun.* **11** 220
- Yu N, Gao L, Zhao S and Wang Z 2009 *Electrochim. Acta* **54** 3835
- Gyuk I 2004 "Supercapacitors for Electric Storage: Scope and Projects," *Proc. Advanced Capacitor World Summit, July 14-16*, Washington, DC
- Buiel E 2006 "Development of Lead-Carbon Hybrid Battery/Super capacitors," *Proc. Advanced Capacitor World Summit, July 17-19*, San Diego, CA
- Kazaryan S 2007 "Characteristics of the PbO₂|H₂SO₄|C ECs by Universal Supercapacitor, LLC," *Proc. Advanced Capacitor World Summit, July 23-25*, San Diego, CA
- Belyakov A I 2008 "Asymmetric Electrochemical Supercapacitors with aqueous electrolytes", *ESSCAP, Novemeber 6-7*, Roma, Italy.
- Kazaryan S A, Litvinenko S V and Kharisov G G 2008 *J. Electrochem. Soc.* **155** 464
- Shukla A K, Ravikumar M K and Gaffoor S A International Patent WO 2011/161686 A1
- Shukla A K, Banerjee A, Ravikumar M K and Gaffoor S A 2011 *2441/CHE/2011/July 18*
- Vijayamohan K, Sathyanarayana S and Joshi S N 1989 *J. Power Sources* **27** 167
- Conway B E 1999 *Electrochemical supercapacitors, scientific fundamentals and technological applications* (New York: Kluwer Academic/ Plenum Publishers)
- Zheng J P, Huang J and Jow T R 1997 *J. Electrochem. Soc.* **144** 2026
- Petersson I, Ahlberg E and Berghult B 1998 *J. Power Sources* **76** 98
- Ganguly P and Hegde M S 1988 *Phys. Rev. B* **37** 5109

17. Sing S W, Everett D H, Haul R A W, Moscou L, Pierotti R A, Rouquerol J and Siemieniewska T 1985 *Pure Appl. Chem.* **57** 603
18. Mathias J and Wannemacher G 1988 *J. Colloid Interface Sci.* **125** 61
19. Khan S A, Baker G L and Colson S 1994 *Chem. Mater.* **6** 2359
20. Morita M, Kaigaishi T, Yoshimoto N, Egashira M and Aida T 2006 *Electrochem. Solid-State Lett.* **9** A386-A389
21. Visscher W 1976/77 *J. Power Sources* **1** 257
22. Brezesinski T, Wang J, Polleux J, Dunn B and Tolbert S H 2009 *J. Am. Chem. Soc.* **131** 1802
23. Wang J, Polleux J, Lim J and Dunn B 2007 *J. Phys. Chem. C* **111** 14925
24. Hammon C H, Hamnett A and Vielstich W 1998 *Electrochemistry*, Wiley-VCH pp110
25. Dietz H, Garche J and Wiesener K 1985 *J. Power Sources* **14** 305
26. Burke A 1991 "Laboratory Testing of High Energy Density Capacitors for Electric Vehicles", EG & G Idaho. Inc., Report No. EGG-EP-9885